Assessment of a flame surface density-based subgrid turbulent combustion model for nonpremixed flames of wood pyrolysis gas

Xiangyang Zhou[a)]
Department of Mechanical Engineering, University of California, Riverside, California 92521

Watit Pakdee
Department of Mechanical Engineering, University of Colorado at Boulder, Boulder, Colorado 80309

Shankar Mahalingam
Department of Mechanical Engineering, University of California, Riverside, California 92521

A flame surface density (FSD) model for closing the unresolved reaction source terms is developed and implemented in a large eddy simulation (LES) of turbulent nonpremixed flame of wood pyrolysis gas and air. In this model, the filtered reaction rate $\bar{\omega}_\alpha$ of species α is estimated as the product of the consumption rate per unit surface area m_α and the filtered FSD $\bar{\Sigma}$. This approach is attractive since it decouples the complex chemical problem (m_α) from the description of the turbulence combustion interaction ($\bar{\Sigma}$). A simplified computational methodology is derived for filtered FSD $\bar{\Sigma}$, which is approximated as the product of the conditional filtered gradient of mixture fraction and the filtered probability density function. Two models for flamelet consumption rate m_α are proposed to consider the effect of filtered scalar dissipation rate. The performance of these models is assessed by direct numerical simulation (DNS) database where a laminar diffusion flame interacts with a decaying homogeneous and isotropic turbulent flow field. The chemistry is modeled by a four-step reduced mechanism that describes the oxidization process of gaseous fuel released from high temperature pyrolysis of wood occurring in a wildland fire. Two-dimensional (2D) and 3D LES computations based on the FSD models are conducted for the same conditions as the DNS. The comparative assessments confirm the applicability of the proposed FSD model to describe the filtered reaction rate and the time evolution of temperature and species concentration in the turbulent nonpremixed flame. © *2004 American Institute of Physics.* [DOI: 10.1063/1.1778371]

I. INTRODUCTION

Turbulent nonpremixed flame is an important ingredient in many engineering applications such as energy production and fire safety. In a "nonpremixed" regime, the fuel and oxidizer are initially unmixed, and in order for chemical reaction to take place, they must first mix together. The rates at which fuel and oxidizer are consumed, and at which heat and product species are produced, are controlled, to a large extent by mixing. In most instances the flow in which the combustion takes place is turbulent. Furthermore, the combustion process itself is usually described by a very large system of elementary chemical reactions. These chemical kinetic mechanisms are often extremely stiff and involve hundreds of chemical species. The governing equations describing the chemical composition are closely coupled to those describing the turbulent transport, and the chemical reaction rates are nonlinear and strongly dependent on the instantaneous composition and temperature.

A significant role of direct numerical simulations (DNS) of turbulent flames is to assess the importance of various physical mechanisms such as transient, differential diffusion, heat release, and curvature effects.[1–4] In DNS, all of the relevant flow and reactive scales are resolved and, therefore, no closure model is needed. With current computer limitations, however, DNS can only be applied to low Reynolds number flows with relatively small range of scales, but those are often insufficient in real flow and combustion problems. Large eddy simulation (LES), which involves DNS of the large-scale turbulence and modeling of the small-scale turbulence, is regarded as a promising tool available today for numerical simulation of turbulent flame.[5–8] Nevertheless, a difficulty occurs in developing subgrid scale (SGS) reaction models for turbulent flame because the reaction region is generally too thin to be resolved on the computational grid. Several models have been proposed to achieve chemical closure, but many of these are still applicable to limited flow or chemistry regimes.

One model of turbulent reactive flow that accounts for real chemical kinetics is the laminar flamelet model.[9] In these models, chemical reactions are assumed to take place along a flamelet interface that is thinner than the smallest turbulent length scale. There has been considerable work on this type of model for LES of nonpremixed combustion.[10–12]

Another means of closing the chemical source term is to solve the transport equation for the joint probability density function (PDF) of the composition vector.[13] The use of PDF for LES was suggested by several authors and has proven to

[a)]Author to whom correspondence should be addressed. Telephone: (909) 787-6428; fax: (909) 787-2899; electronic mail: xzhou@engr.ucr.edu

be useful.[14–16] This is partly due to the distinct advantage of PDF over moment methods that the effects of chemical reaction appear in a closed form, although the mixing term in the transport equations is unclosed and must be modeled.

Based on the conditional moment closure method,[17,18] in which the conditional average of the chemical source term can be modeled by evaluating the chemical reaction rates using the conditional averages of the composition vector and temperature, a conditional source-term estimation method was proposed to close the chemical source terms for LES of nonpremixed reacting flows.[19] The results obtained are in reasonable agreement with available experimental data.

As an important aspect of turbulent reaction models, several authors have proposed closure models of the reaction rate term based on the flame surface density (FSD) concept. These models also assume that chemical reactions occur in thin layers called flamelets. This regime of combustion prevails when the chemical time scales are smaller than the turbulence time scales. From phenomenological considerations, Marble and Broadwell[20] first proposed the coherent flame model to describe nonpremixed turbulent combustion, in which the Reynolds averaged reaction rate $\langle \dot{\omega} \rangle_\alpha$ is modeled as the product of the local reaction rate per unit of flame area, m_α, and the averaged FSD $\langle \Sigma \rangle$ (i.e., the available flame surface per unit volume). This approach is attractive because it decouples the chemical problem (m_α) from the description of the turbulence combustion interaction ($\langle \Sigma \rangle$).

In these models based on FSD concept, there are two unknown parameters: m_α and $\langle \Sigma \rangle$. The estimates of these two terms are equally important, and are the topic of the current study. A local model provides the flamelet consumption rate m_α. This quantity is generally estimated from counterflow strained laminar flame calculations. The mean FSD is estimated from a phenomenological balance equation, first proposed by Marble and Broadwell.[20] Using the formalism proposed by Pope,[21] Vervisch et al.[22] have obtained exact transport equation for the isolevel surface density of any quantity governed by a balance equation. The similarity between PDF and flame surface models was thus made evident. Extending the displacement speed definition proposed by Vervisch et al.[22] to nonpremixed combustion, an exact transport equation has been obtained by Van Kalmthout and Veynante[23] for the diffusion flame surface density. Using DNS of a spatially developing turbulent reacting mixing layer, FSD concept was found to provide a relevant description for nonpremixed turbulent combustions.

Extending the FSD concept to LES of turbulent nonpremixed flames, it is useful to examine the ability of spatially filtered FSD $\bar{\Sigma}$ to describe the filtered reaction rate $\bar{\omega}_\alpha$, where the overbar (–) denotes spatial filtered value. This is an open question that has not been investigated extensively for turbulent nonpremixed flames. However, it is noted that several studies have examined this in the context of turbulent premixed flames.[24–26] In a recent work of Zhou and Mahalingam,[27] a combustion model based on this FSD concept was developed and implemented in a two-dimensional (2D) LES of turbulent nonpremixed combustion. In this model, the filtered reaction rate $\bar{\omega}_\alpha$ of species α is estimated

as the product of the consumption rate per unit surface area m_α and the filtered FSD $\bar{\Sigma}$ as

$$\bar{\omega}_\alpha(x,t) = m_\alpha \bar{\Sigma}(x,t). \tag{1}$$

The filtered FSD is modeled as the product of the conditional filtered gradient of mixture fraction and the filtered probability density function. With validation provided by DNS data, the calculated LES results showed that the proposed FSD model provides a good description of the filtered reaction rate.

This work extends the preliminary analysis of Zhou and Mahalingam[27] on a FSD based turbulent combustion model to an extensive a priori and a posteriori assessment in a larger computational domain. A detailed basis for the model is developed. Following this discussion, the performance of the proposed FSD models is assessed by a 2D DNS database where a laminar diffusion flame interacts with a decaying homogeneous and isotropic turbulent flow field. A 3D LES computation based on FSD models is conducted by utilizing a parallel computing system. For the long-term purpose of developing a physically based predictive capability for wildland fire spread, turbulent nonpremixed combustion between wood pyrolysis gas and air is investigated. In an intense wildfire, fuel supply to largely gaseous flames is mainly a result of pyrolysis of cellulose present in vegetation. Gaseous fuel released from high temperature pyrolysis of ground fuel is a complex and highly variable mixture, which includes four main gases: carbon monoxide (CO), hydrogen (H_2), methane (CH_4), and carbon dioxide (CO_2).[28] Although a detailed reaction mechanism to accurately describe the complex chemistry is possible, the computational costs are exceptionally expensive and not practical. Therefore a recently derived reduced four-step chemical kinetic scheme is used to model the chemical reaction of wood pyrolysis gas.[29] In Sec. II, the governing equations and models implemented for various terms arising in a LES are described. The filtered FSD-based model and associated submodels are described in detail in Sec. III. Section IV is dedicated to the description of the numerical methods applied in DNS and LES of turbulent nonpremixed flame. Results of filtered FSD and reaction rate obtained from 2D and 3D computations are presented in Sec. V where the proposed FSD-based model is assessed.

II. GOVERNING EQUATIONS

Here we consider a compressible turbulent reactive flow involving N_s species. The Navier–Stokes equations in standard Cartesian tensor form are

$$\frac{\partial \rho}{\partial t} + \frac{\partial \rho u_i}{\partial x_i} = 0, \tag{2}$$

$$\frac{\partial \rho u_i}{\partial t} + \frac{\partial \rho u_i u_j}{\partial x_j} = \frac{\partial \tau_{ij}}{\partial x_j} - \frac{\partial p}{\partial x_i}, \tag{3}$$

$$\frac{\partial \rho Y_\alpha}{\partial t} + \frac{\partial \rho u_j Y_\alpha}{\partial x_j} = \frac{\partial}{\partial x_j}\left(\rho D_\alpha \frac{\partial Y_\alpha}{\partial x_j}\right) + W_\alpha \omega_\alpha, \tag{4}$$

Phys. Fluids, Vol. 16, No. 10, October 2004

Assessment of a flame surface density-based model 3797

$$\frac{\partial \rho e_t}{\partial t} + \frac{\partial (\rho e_t + p) u_j}{\partial x_j} = \frac{\partial u_j \tau_{kj}}{\partial x_k} - \frac{\partial q_j}{\partial x_j}, \tag{5}$$

where ρ, u_j, p, Y_α, and e_t are the density, velocity vector, pressure, mass fraction of species α, and total specific energy, respectively. The symbols x_i and t denote position vector and time. The total specific energy is given by

$$e_t = e + \tfrac{1}{2} u_k u_k, \tag{6}$$

where $e = \Sigma_{\alpha=1}^{N_s} Y_\alpha h_\alpha - p/\rho$ and $h_\alpha = h_{f,\alpha}^0 + \int_{T_0}^{T} c_{p,\alpha}(T') dT'$ with h_α denoting the enthalpy of species α, include the enthalpy of formation and the temperature-dependent sensible enthalpy. The viscous stress tensor τ_{ij} and heat flux vector q_j are given by

$$\tau_{ij} = \mu \left(\frac{\partial u_i}{\partial x_j} + \frac{\partial u_j}{\partial x_i} - \frac{2}{3} \frac{\partial u_k}{\partial x_k} \delta_{ij} \right) \tag{7}$$

and

$$q_j = -\lambda \frac{\partial T}{\partial x_j} - \rho \sum_{\alpha=1}^{N_s} h_\alpha D_\alpha \frac{\partial Y_\alpha}{\partial x_j}, \tag{8}$$

respectively, where μ, λ, and D_α denote the mixture dynamic viscosity, thermal conductivity, and species diffusivity. An ideal gas is assumed and the equation of state is $p = \rho R T$, where $R = R^0 \Sigma_{\alpha=1}^{N_s} Y_\alpha / W_\alpha$, R^0 is the universal gas constant, and W_α is the molecular weight of species α.

Large eddy simulation involves use of the spatial filtering operation,

$$\bar{f}(x,t) = \int_{-\infty}^{\infty} f(x',t) G(x' - x) dx', \tag{9}$$

where $G(x)$ is the filter function. Considering the variable density case, the filtered quantity is density weighted,

$$\langle f(x,t) \rangle_F = \overline{\rho f} / \bar{\rho}, \tag{10}$$

where $\langle f \rangle_F$ denotes the Favre filtered variable and $f'' = f - \langle f \rangle_F$ denotes the fluctuation from the Favre filtered value. Filtering the governing equations, we obtain

$$\frac{\partial \bar{\rho}}{\partial t} + \frac{\partial \bar{\rho} \langle u_i \rangle_F}{\partial x_i} = 0, \tag{11}$$

$$\frac{\partial \bar{\rho} \langle u_i \rangle_F}{\partial t} + \frac{\partial \bar{\rho} \langle u_i \rangle_F \langle u_j \rangle_F}{\partial x_j} + \frac{\partial \bar{p}}{\partial x_i} = \frac{\partial \bar{\tau}_{ij}}{\partial x_j} - \frac{\partial \sigma_{ij}}{\partial x_j}, \tag{12}$$

$$\frac{\partial \bar{\rho} \langle Y_\alpha \rangle_F}{\partial t} + \frac{\partial \bar{\rho} \langle u_j \rangle_F \langle Y_\alpha \rangle_F}{\partial x_j} = \frac{\partial}{\partial x_j} \left(\overline{\rho D_{\alpha,N} \frac{\partial Y_\alpha}{\partial x_j}} \right) - \frac{\partial M_j^\alpha}{\partial x_j}$$
$$+ W_\alpha \bar{\omega}_\alpha, \tag{13}$$

$$\frac{\partial (\bar{\rho} \langle e_t \rangle_F + k)}{\partial t} + \frac{\partial [(\bar{\rho} \langle e_t \rangle_F + \bar{p}) \langle u_j \rangle_F + K_j + Q_j]}{\partial x_j}$$
$$= \frac{\partial \overline{u_i \tau_{ji}}}{\partial x_j} - \frac{\partial \bar{q}_j}{\partial x_j}, \tag{14}$$

where $\quad \langle e_t \rangle_F = \langle e \rangle_F + \tfrac{1}{2} \langle u_k \rangle_F \langle u_k \rangle_F \quad$ and $\quad k = \tfrac{1}{2} \bar{\rho} \langle u_k u_k \rangle_F$

$-\tfrac{1}{2} \bar{\rho} \langle u_k \rangle_F \langle u_k \rangle_F$. The filtered ideal gas equation of state is $\bar{p} = \overline{\rho R T} = \bar{\rho} \langle R \rangle_F \langle T \rangle_F$.

The molecular viscous and diffusive fluxes in the momentum, species, and energy equations need special treatment. Using low Reynolds number DNS data of isotropic turbulence at several Mach numbers, it was found that the subgrid scale contribution arising from the nonlinearities in the molecular viscous and diffusive fluxes are small when compared to convective turbulent subgrid-scale terms given by the above equations.[30] These contributions and the k term in Eq. (14) were omitted in the present preliminary investigation.

The filtered molecular viscosity is assumed to be a function of the filtered temperature following a power law, where again the subgrid scale fluctuations of the temperature are neglected,[31]

$$\langle \mu \rangle_F \approx \mu_0 (\langle T \rangle_F / T_0)^{0.6756}. \tag{15}$$

A constant Prandtl number Pr=0.7 is used in thermal conductivity. However, different molecular Schmidt numbers were assumed for species,

$$Sc_\alpha = \frac{\langle \mu \rangle_F}{\bar{\rho} \langle D_{\alpha,N} \rangle_F}. \tag{16}$$

The filtered mean specific heat at the constant pressure is assumed to be a function of the filtered temperature and filtered species mass fraction, where the subgrid scale fluctuations of the temperature and species are neglected,

$$\langle c_p \rangle_F = \sum_{\alpha=1}^{N_s} \langle Y_\alpha \rangle_F c_{p,\alpha}(\langle T \rangle_F). \tag{17}$$

The following unresolved subgrid scale convective fluxes of momentum, species, and energy:

$$\sigma_{ij} = \bar{\rho} \langle u_i u_j \rangle_F - \bar{\rho} \langle u_i \rangle_F \langle u_j \rangle_F, \tag{18}$$

$$M_j^\alpha = \bar{\rho} \langle u_j Y_\alpha \rangle_F - \bar{\rho} \langle u_j \rangle_F \langle Y_\alpha \rangle_F, \tag{19}$$

$$K_j = \tfrac{1}{2} \bar{\rho} \langle u_k u_k u_j \rangle_F - \tfrac{1}{2} \bar{\rho} \langle u_k \rangle_F \langle u_k \rangle_F \langle u_j \rangle_F, \tag{20}$$

$$Q_j \approx \bar{\rho} \langle c_p \rangle_F (\langle T u_j \rangle_F - \langle T \rangle_F \langle u_j \rangle_F), \tag{21}$$

need to be modeled. We make use of currently available closures, which are well established in turbulent flows.[32] The subgrid stress can be modeled using a variable density form of the Smagorinsky model as

$$\sigma_{ij} = -2 C_R \Delta^2 \bar{\rho} \sqrt{\Pi} \left(\langle S_{ij} \rangle_F - \tfrac{1}{3} \langle S_{kk} \rangle_F \delta_{ij} \right) + \tfrac{2}{3} C_I \Delta^2 \bar{\rho} \Pi \delta_{ij}, \tag{22}$$

where

$$\langle S_{ij} \rangle_F = \frac{1}{2} \left(\frac{\partial \langle u_i \rangle_F}{\partial x_j} + \frac{\partial \langle u_j \rangle_F}{\partial x_i} \right) \quad \text{and} \quad \Pi = \langle S_{kl} \rangle_F \langle S_{kl} \rangle_F. \tag{23}$$

The variable Δ is the filter width, and the corresponding subgrid eddy viscosity is

$$\mu_t = C_R \Delta^2 \bar{\rho} \sqrt{\Pi}. \tag{24}$$

The numerical values of C_R and C_I depend on how Δ^2 is defined. In the work of Ragab and Sheen, Δ^2 is defined as $\Delta^2 = ((\Delta x)^2 + (\Delta y)^2 + (\Delta z)^2)/3$, $C_R = 0.05$ and $C_I = 0.01$.[32] A similar model is used for the closure of the subgrid scalar mass flux,

$$M_j^\alpha = -\Gamma_t \frac{\partial \langle \phi_\alpha \rangle_F}{\partial x_j}, \tag{25}$$

where $\Gamma_t = \mu_t / Sc_t$, and Sc_t is the subgrid Schmidt number and is assumed to be a constant. The temperature-velocity correlation terms are modeled by a gradient-transport model,

$$Q_j = -\frac{\langle c_p \rangle_F \mu_t}{Pr_t} \frac{\partial \langle T \rangle_F}{\partial x_j}, \tag{26}$$

where Pr_t is the subgrid scale Prandtl number. The convective transfer of subgrid scale kinetic energy is approximated as

$$K_j = \sigma_{ij} \langle u_j \rangle_F. \tag{27}$$

The modeling of the filtered reaction rate term $\bar{\omega}_\alpha$ in Eq. (13) for LES of nonpremixed turbulent flame is the subject of the flame surface density based turbulent combustion approach as described in the following section.

III. FLAME SURFACE DENSITY BASED TURBULENT COMBUSTION MODEL

The major stumbling block for introducing LES to reacting flow problems is the proper modeling of the reaction source terms. The focus of this paper is to use the FSD concept to model reaction source terms via Eq. (1). In order to better understand the rationale for this model, consider a one-dimensional diffusion flame configuration as depicted in Fig. 1 which is calculated using OPPDIF code for wood pyrolysis gas and air.[33] The filtered reaction rate is given by

$$\bar{\omega}_\alpha(x,t) = \int_0^L \omega_\alpha(x',t) G(x-x') dx' = \frac{1}{L} \int_0^L \omega_\alpha(x',t) dx', \tag{28}$$

where the filter function G is of the form

$$G(x-x') = \begin{cases} \dfrac{1}{L} & |x'-x| \leq \dfrac{L}{2} \\ 0 & \text{otherwise}, \end{cases} \tag{29}$$

where L, assumed larger than flame thickness, is the length scale over which the averaging is carried out.

Under the flamelet assumption, the diffusion flame is located near the stoichiometric isolevel of mixture fraction Z_{st}. Since the flame front in diffusion flames corresponds to a particular isolevel of the passive scalar, an exact expression for the instantaneous FSD arises from the general definition of the surface density of Z_{st} isolevel,[21-23]

$$\Sigma(x,t) = |\nabla Z(x,t)| \delta[Z_{st} - Z(x,t)], \tag{30}$$

where δ is the Dirac delta function, and the filtered FSD is determined by
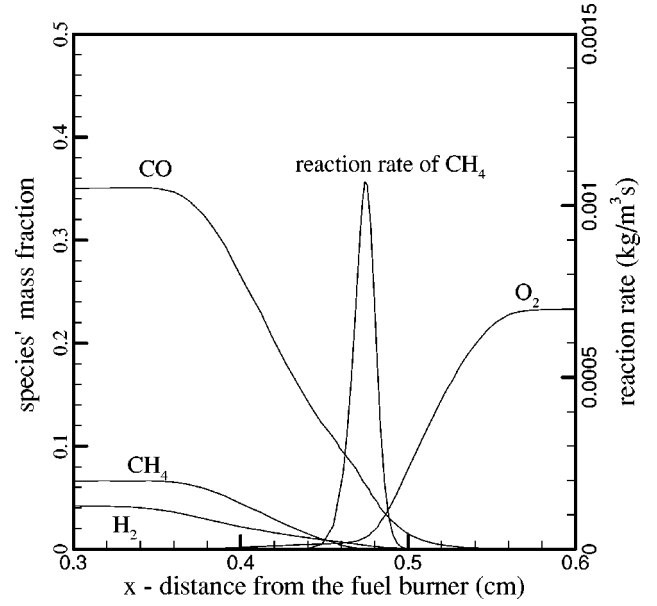
FIG. 1. The mass fractions of fuel (a mixture of three reactants: CH_4, CO, and H_2) and oxidizer (O_2), and the reaction rate profile of CH_4 in a 1D laminar diffusion flame, which is also used as the initial condition by DNS and LES computation.

$$\bar{\Sigma}(x,t) = \int_0^L |\nabla Z(x',t)| \delta[Z_{st} - Z(x',t)] G(x'-x) dx'. \tag{31}$$

Based on the property of δ for small ΔZ,

$$\int_{Z_{st}-\Delta Z/2}^{Z_{st}+\Delta Z/2} \delta(Z_{st} - Z) dZ = 1, \tag{32}$$

then using an approximation of $\delta(Z_{st} - Z) \approx 1/\Delta Z$, a simple numerical estimate for filtered FSD [Eq. (31)] can be expressed as

$$\bar{\Sigma}(x,t) \approx \sum_{i=1}^n \frac{\Delta Z}{\Delta x'} \frac{1}{\Delta Z} \frac{1}{L} \Delta x' = \frac{1}{L}, \tag{33}$$

where n is the number of discrete, uniformly spaced sample points. The flamelet consumption rate obtained from a one-dimensional unstrained diffusion flame has the form[23]

$$m_\alpha = \int_0^1 \omega_\alpha(x',t)/(\chi/2D)^{1/2} dZ, \tag{34}$$

where $\chi = 2D |\nabla Z|^2$. From the above definition, the consumption rate for one-dimensional case can be approximated as

$$m_\alpha \approx \int_0^L \dot{\omega}_\alpha(x',t) dx'. \tag{35}$$

From Eqs. (33) and (35), we have $m_\alpha \bar{\Sigma}(x',t) = (1/L) \int_0^L \omega_\alpha(x',t) dx' = \bar{\omega}_\alpha(x,t)$. For a simple one-dimensional laminar diffusion flame, this is consistent with the proposed model of filtered reaction rate given in Eq. (1).

For LES of turbulent nonpremixed flame, because of the effect of turbulent mixing, both of the terms $\bar{\Sigma}$ and m_α need to be modeled separately. This is the topic of the present

work. At first a simple model developed for $\bar{\Sigma}$ is illustrated in Sec. III A, and then two models for m_α are proposed and analyzed in Sec. III B.

A. Model for the filtered FSD

The transport equation for filtered FSD $\bar{\Sigma}$ can be obtained by filtering the exact transport equation of the instantaneous Σ proposed by Van Kalmthout and Veynante.[23] However, this equation needs closure models for several terms corresponding to tangential strain rate acting on the flame surface, a term combining molecular diffusion and curvature effects, and a flux term through the isolevels of Z. This may make the approach of utilizing the transport equation for $\bar{\Sigma}$ difficult. As pointed out by Vervisch et al.,[22] there are similarities between the FSD and PDF. Here we propose to use PDF to model FSD. Application of the filtering operation to the exact definition of the FSD yields

$$\bar{\Sigma}(x,t) = \overline{|\nabla Z(x,t)|}_{st} P_L(Z_{st};x,t), \tag{36}$$

where $\overline{|\nabla Z(x,t)|}_{st}$ is defined by Colucci et al.[15] as the conditional filtered value of the passive scalar gradient along the isosurface $Z(x,t)=Z_{st}$. Pope[34] introduced the concept of filtered density function (FDF) that is essentially the PDF of SGS scalar variables. For that, PL is defined as

$$P_L(Z_{st};x,t) = \int_{-\infty}^{\infty} \delta[Z_{st} - Z(x',t)]G(x'-x)dx'. \tag{37}$$

With the condition of a positive filter kernel, PL has all the properties of the PDF. It implies that the filtered FSD can be calculated from conditional filtered gradient and FDF.

The FDF can be obtained by solving the transport equation proposed by Colucci et al.[15] but this equation needs other closure hypotheses and can significantly increase the computational cost. For the purpose of the application of FSD approach in the current LES, a less expensive solution is to presume this FDF according to its two first moments ($\bar{Z}$ and $\overline{Z^2}$) and the β function,[10]

$$P_L(Z;x,t) = \frac{Z^{a-1}(1-Z)^{b-1}}{B(a,b)}, \tag{38}$$

where

$$a = \bar{Z}\left[\frac{\bar{Z}(1-\bar{Z})}{Z_v^2} - 1\right], \quad b = \frac{a}{\bar{Z}} - a, \quad Z_v^2 = \overline{Z^2} - \bar{Z}^2. \tag{39}$$

The quantity $B(a,b)$ is the β function and Z_v^2 is the subgrid scale variance of Z evaluated using a scale similarity model,[10]

$$Z_v^2 = \overline{Z^2} - \bar{Z}^2 = C_f(\overline{\bar{Z}^2} - \bar{Z}^2), \tag{40}$$

where the overbar $\rightarrow$ corresponds to the test filter with a size wider than the size of the mesh. The scale similarity constant C_f was determined from the DNS data.

B. Model for the flamelet consumption rate

A model for the flamelet consumption rate m_α was proposed previously as[27]

$$m_\alpha = m_\alpha(\bar{\chi}_{st}). \tag{41}$$

Then there remains the problem of modeling the conditional filtered scalar dissipation rate $\bar{\chi}_{st}$ and the conditional filtered mixture fraction gradient $\overline{|\nabla Z(x,t)|}_{st}$. The functional dependence of χ on Z applicable to a laminar counterflow diffusion flame is given as[10]

$$\chi = \chi_0 \exp(-2[\mathrm{erfc}^{-1}(2Z)]^2) = \chi_0 F(Z), \tag{42}$$

where χ_0 is the local peak of χ within the diffusion layer, and erfc^{-1} is the inverse error function. Cook et al.[10] assume that the same dependence of $\bar{\chi}_Z$ on Z as in Eq. (42) is valid. The conditional filtered scalar dissipation rate $\bar{\chi}_Z$ is related to that at a fixed value, say Z_{st}, by

$$\bar{\chi}_Z = \bar{\chi}_{st} \frac{F(Z)}{F(Z_{st})}. \tag{43}$$

Then with the presumed FDF $P_L(Z)$ being known, the unconditional filtered average can be written as

$$\bar{\chi} = \int_0^1 \bar{\chi}_Z P_L(Z)dZ = \bar{\chi}_{st} \int_0^1 \frac{F(Z)}{F(Z_{st})} P_L(Z)dZ. \tag{44}$$

Therefore the conditional filtered scalar dissipation rate $\bar{\chi}_{st}$ can be expressed as

$$\bar{\chi}_{st} = \frac{\bar{\chi}F(Z_{st})}{\int_0^1 F(Z)P_L(Z)dZ}. \tag{45}$$

Using the model proposed by de Bruyn Kops et al.,[11] the unconditional filtered average $\bar{\chi}$ can be modeled as

$$\bar{\chi} = 2\left(\frac{\bar{\mu}}{\bar{\rho}\mathrm{Sc}} + \frac{\mu_t}{\bar{\rho}\mathrm{Sc}_t}\right)|\nabla \bar{Z}|^2, \tag{46}$$

where the subscript t denotes the subgrid value of viscosity μ and Schmidt number Sc.

The gradient magnitude $|\nabla Z|$ is also the function of Z. Following the same method for χ, a model for the conditional filtered gradient $\overline{|\nabla Z(x,t)|}_{st}$ was developed. Analogous to Eq. (42), the functional dependence of $|\nabla Z|$ on Z can be expressed as

$$|\nabla Z| = |\nabla Z|_0 \exp(-[\mathrm{erfc}^{-1}(2Z)]^2) = |\nabla Z|_0 H(Z). \tag{47}$$

Following the assumption of Cook et al.[10] we obtain

$$\overline{|\nabla Z|}_Z = \overline{|\nabla Z|}_{st} \frac{H(Z)}{H(Z_{st})}, \tag{48}$$

$$\overline{|\nabla Z|}_{st} = \frac{\overline{|\nabla Z|}H(Z_{st})}{\int_0^1 H(Z)P_L(Z)dZ}. \tag{49}$$

Here the unconditional filtered gradient $\overline{|\nabla Z|}$ can be approximated through the unconditional filtered scalar dissipation rate $\bar{\chi}$ as

$$\overline{|\nabla Z|} = (\overline{\chi}/2\overline{D})^{0.5}, \tag{50}$$

where $\overline{D}$ is the filtered species diffusion coefficient.

A library of flamelet consumption rate $m_\alpha(\chi_{st})$ was constructed by calculating a counterflow strained laminar flame using OPPDIF code[33] under various strain rates. In order to compute m_α, χ_{st} is parametrized by $\overline{\chi}_{st}$, and $m_\alpha(\overline{\chi}_{st})$ takes the value of $m_\alpha(\chi_{st})$ in the flamelet library. This procedure could lead to errors. The main reason is that the parameter χ_{st} considered in flamelet library is not an averaged value, unlike the parametrized value $\overline{\chi}_{st}$.

Rather than pursuing this procedure, in the present study a simpler approach to model the flamelet consumption rate is proposed as

$$m_\alpha = m_\alpha(\overline{\chi}). \tag{51}$$

In this model, the unconditional average value $\overline{\chi}$ is considered. Therefore, instead of parametrizing χ by $\overline{\chi}_{st}$, the unconditional average value $\overline{\chi}$ is used. Following this approach, a library of $m_\alpha(\overline{\chi})$ for various $\overline{\chi}$ is constructed, in which $\overline{\chi}$ is determined by

$$\overline{\chi} = \frac{\int_0^L \chi dx}{L}, \tag{52}$$

where L is the filter size in the LES. It is worth noting that this model avoids the need for closure of the conditional average scalar dissipation rate, through which an error could be introduced. The effect of this model [Eq. (51)] will be compared against the previous model [Eq. (41)] in Sec. V.

IV. NUMERICAL APPROACH

The chemistry is modeled by a recently developed four-step reduced mechanism that describes the oxidization process of gaseous fuel released from high temperature pyrolysis of wood occurred in wildland fire. The model involved as reacting species CO, H_2, and CH_4, the products H_2O and CO_2, and the radical H as intermediate species. The mass fractions of the pyrolysis fuel gas chosen in this paper are $Y_{CO}=0.35$, $Y_{H_2}=0.042$, $Y_{CH_4}=0.066$, and $Y_{CO_2}=0.542$, representative of the composition of high temperature pyrolysis of Aspen wood.[28] The mixture fraction for the pyrolysis gas mixture is defined as a linear combination of elemental mass fractions of carbon C, hydrogen H, and nitrogen N atoms,[35]

$$Z = \frac{\dfrac{y_C - y_{C,O}}{\nu_C W_C} + \dfrac{y_H - y_{H,O}}{\nu_H W_H} + 2\dfrac{y_{N,O} - y_N}{\nu_N W_N}}{\dfrac{y_{C,F} - y_{C,O}}{\nu_C W_C} + \dfrac{y_{H,F} - y_{H,O}}{\nu_H W_H} + 2\dfrac{y_{N,O} - y_{N,F}}{\nu_N W_N}}, \tag{53}$$

where coefficients ν_C, ν_H, and ν_N denote the elemental numbers of C, H, and N in the global one-step reaction, the W's denote the appropriate atomic weights, and the second subscript O and F denote the initially unmixed oxidizer and fuel states, respectively. With this definition of mixture fraction, the peak temperature is very close to stoichiometric over a range of pyrolysis gas composition. The stoichiometric mix-
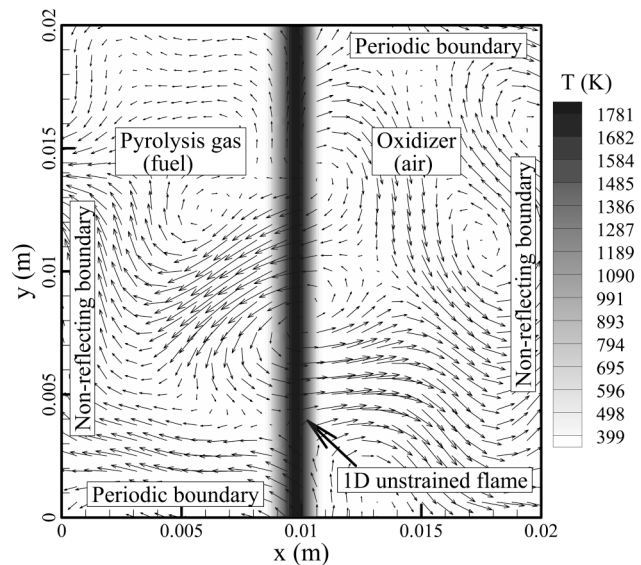
FIG. 2. Schematic representation of initial temperature and turbulent flow field with given boundary conditions.

ture fraction for the chosen pyrolysis gas composition burning with air is $Z_{st}=0.226$.

An initially strained, one-dimensional laminar diffusion flame, between pyrolysis gas mixture and air, computed using OPPDIF code,[33] is used for the reaction zone initialization (Fig. 1). Once the strain is removed, the solution is evolved until the weak initial disturbance acoustic waves exit the domain. At this stage, the only velocity is that induced by the flame. The reaction zone thickness is defined as the distance over which the reaction rate changes from 10% of its peak value back to this same value. Periodic boundary conditions along the lateral boundaries and nonreflecting boundary conditions at the other two boundaries are implemented. A schematic representation of the computational domain and initial contours of temperature are given in Fig. 2.

An initial turbulent flow field is also illustrated in Fig. 2 by plotting velocity vectors. This homogeneous turbulence field is initialized in the computational domain after the initial disturbance acoustic waves exit the domain. The turbulent velocity field is generated according to the turbulent kinetic energy spectrum function

$$E(k) = C_0 \frac{u_{rms}^2}{k_0}\left(\frac{k}{k_0}\right)^4 \exp\left[-2\left(\frac{k}{k_0}\right)^2\right], \tag{54}$$

where k is the wave number, and C_0 is a constant. The wave number k_0 corresponds to the maximum $E(k)$ which relates to the most energetic eddies. The turbulence field is superimposed on the laminar field. The initial turbulent Reynolds number $\mathrm{Re}_{l_t}=u_t l_t/\nu=197$ is introduced where u_t is the initial turbulent velocity, l_t is the initial integral length scale, and ν is the kinematic viscosity. The initial eddy turnover time $t_e = l_t/u_t$ is 0.00422 s.

A compressible DNS code[36] originally developed for combustion of perfect gases with constant specific heats was modified to accurately treat mixture gases having variable thermodynamic properties with complex chemistry. The gov-

erning equations [Eqs. (2)–(5)] are numerically integrated in time using a third-order Runge–Kutta scheme. Spatial derivatives are discretized using a sixth-order accurate compact finite difference scheme on a uniform mesh.[37] Boundary conditions are specified using a recently developed method,[38] which is the modified version of the Navier–Stokes characteristic boundary condition.[39,40] For the present LES computation, same numerical methods were utilized to solve the governing equations [Eqs. (11)–(14)] with the subgrid scale models.

A two-dimensional square computational domain with 2.0×2.0 cm is considered for DNS. The parallel computation was conducted based on a parallel method developed and used for DNS of turbulent stratified shear flow.[41] The two-dimensional problem of N data points is distributed equally in the y-coordinate direction. Derivatives are computed locally in parallel. The derivatives with respect to x can be evaluated without communication, whereas communication between processors is required to evaluate the derivatives with respect to y. Therefore a parallel matrix transpose algorithm is implemented to compute y derivatives locally, and in parallel. The communication that is required is achieved by using message passing interface. For DNS, a two-dimensional computational grid points of 512×512 are distributed equally over eight processors. Each processor then executes a computation on 512×64 grid points. The parallel computations are performed on the UCR-Institute of Geophysics and Planetary Physics (IGPP) Beowulf computer Lupin.

The LES computation with FSD model is conducted on grids coarser than that in DNS. For 2D nonpremixed flame, the LES resolution is 65×65 grid points in a same computational domain with DNS. The LES computation is initiated from a same condition with DNS. Because of reduced grid points, 2D LES can be computed using a serial computer. For 3D case, the computational domain is $2.0 \times 2.0 \times 2.0$ cm with a resolution of $64 \times 64 \times 64$ grid points, where z denotes the spanwise direction. The initial values of the mass fractions of reactants and temperature at each of the spanwise points in 3D are identical to those in 2D. A 3D homogeneous turbulence field is initialized in the computational domain to model the effect of turbulence on a plain laminar diffusion flame surface. The 3D LES is conducted using a parallel computation with eight processors. Each processor executes a computation on $64 \times 64 \times 8$ grid points.

From phenomenological considerations, the FSD may also be defined as the flame surface area δA comprised in a volume δV as[23]

$$\delta A = \int_{\delta V} \Sigma \, dV. \tag{55}$$

This method is useful to estimate the FSD from DNS data. In a two-dimensional configuration, it involves calculation of the flame length δ_l comprised in a mesh of area $\Delta_x \Delta_y$.

V. RESULTS AND DISCUSSION

Using the filtering operation to DNS data, an *a priori* and *a posteriori* validation of a proposed subgrid turbulent
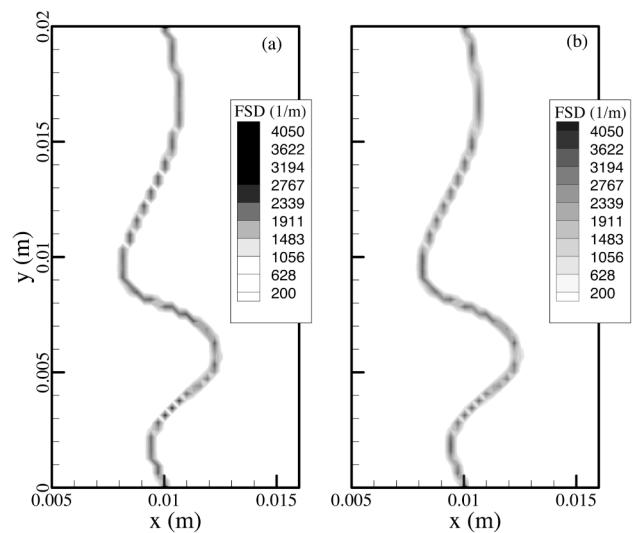
FIG. 3. Comparison of contours of filtered FSD: (a) filtered from DNS data; (b) calculated from the model Eq. (36), at time $t = 0.23 t_e$ and filter size $\Delta_f = 8\Delta_x$.

combustion model based on FSD concept was conducted and is described in the following sections. At first, the filtered value from DNS data is used to demonstrate the effectiveness of filtered FSD model [Eq. (36)] computed from the conditional filtered gradient of mixture fraction and the filtered probability density function. Next the other part of the FSD reactive model, viz., the flamelet consumption rate m_α is examined. Finally *a posteriori* validation is conducted by presenting the results of 2D and 3D LES of nonpremixed turbulent flame using the FSD models developed in this paper.

A. Filtered flame surface density

A physical space tophat filter $G(x)$ with a filter size Δ_f larger than the DNS computational mesh size Δ_x (along the x direction) is used to filter DNS data. With $\Delta_f = 8\Delta_x$, the 512×512 grid over the square domain in the DNS is reduced to 65×65. Figure 3(a) shows instantaneous FSD contours of $\bar{\Sigma}_d(x,t)$ computed by filtering the DNS data at $t = 0.23 t_e$, where t_e is the initial eddy turnover time. With time evolution, the initially planar laminar flame (see Fig. 2) is stretched and distorted by the turbulence. The total flame surface area is increased. Figure 3(b) shows the predicted contours $\bar{\Sigma}_m(x,t)$, obtained via the model equation [Eq. (36)] using the filtered variables. In general, the FSD contours obtained from the model agree well with that from DNS data. The modeled FSD contours look thicker and smoother than that filtered from DNS. The maximum predicted value of $\bar{\Sigma}_m(x,t)$ is about 3500 m^{-1}, which is smaller than 4050 m^{-1} obtained from DNS. As shown in the following analysis, however, the total flame areas between both are almost same. As the flame front is distorted by the turbulent motions, Fig. 3 shows that the value of $\bar{\Sigma}_d(x,t)$ and $\bar{\Sigma}_m(x,t)$ change in regions where the flame front is curved. This reflects the effect of turbulence on the flame surface area.

Corresponding to Fig. 3, Fig. 4 shows the time evolution
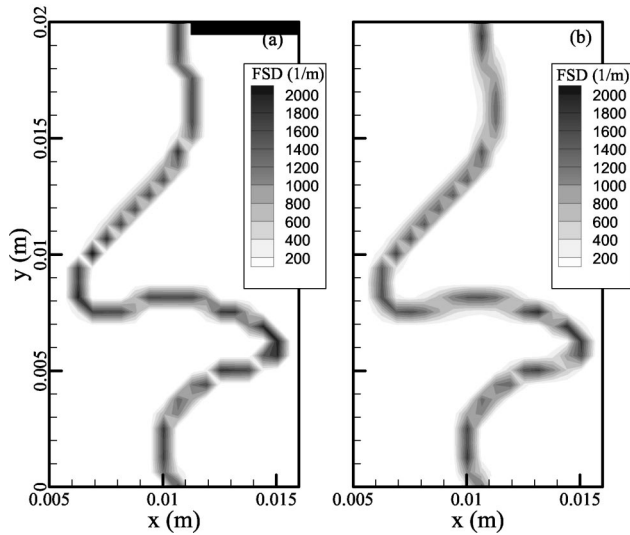
FIG. 4. Comparison of contours of filtered FSD: (a) filtered from DNS data; (b) calculated from the model Eq. (36), at time $t=0.55t_e$ and filter size $\Delta_f = 16\Delta_x$.

FIG. 5. Scatter plots of instantaneous filtered FSD calculated from FSD model vs the exact FSD filtered from DNS at $t=0.55t_e$ and $\Delta_f=16\Delta_x$.

of FSD and the effect of the filter size on FSD. At time $t=0.55\ t_e$ and filter size $\Delta_f=16\Delta_x$, the contours of $\bar{\bar{\Sigma}}_d(x,t)$ are more distorted by turbulent motion [see Fig. 4(a)]. Because FSD is computed with a larger filter size, the thickness of FSD contours is increased and the maximum value is reduced to about 2010 m^{-1}. Figure 4(b) shows the predicted contours of $\bar{\bar{\Sigma}}_m(x,t)$ at the same time and filter size. The maximum value of $\bar{\bar{\Sigma}}_m(x,t)$ is about 1830 m^{-1}. Overall, the comparison is very good, showing that the time evolution of the FSD is predicted quite accurately by the model.

Further validation of the modeled FSD $\bar{\bar{\Sigma}}_m(x,t)$ is carried out by examining quantitatively the computed (via DNS) and predicted (via model) FSD. At the same condition as with Fig. 4 ($t=0.55t_e$ and $\Delta_f=16\Delta_x$), Fig. 5 shows a scatter plot of the instantaneous filtered FSD $\bar{\bar{\Sigma}}_m(x,t)$ versus the exact FSD $\bar{\bar{\Sigma}}_d(x,t)$ filtered from DNS. In general, the magnitudes of actual and modeled FSD agree well. For the value of FSD larger than 1000, the modeled FSD is a little smaller than the actual one, and the opposite case appears in the region where the value of FSD is smaller than 1000. This explains why the modeled FSD contours shown in Figs. 3 and 4 look a little thicker and smoother, and the maximum value is lower. In fact, the thickness of the modeled FSD contours is mainly controlled by FDF because it gives the probability density of flame surface with the condition $\bar{Z}(x,t)=Z_{st}$. FDF also reflects the effect of filter size and turbulent motion on the FSD.

Finally, the integrated FSD Ξ, obtained by integrating across the flame along the x direction

$$\Xi = \frac{1}{L}\int_L \bar{\bar{\Sigma}}(x',t)dx', \tag{56}$$

is plotted in Fig. 6 as a function of y location. Here L is the domain size in x. Integrated FSD is a measure of the mean flame surface density at each horizontal section correspond-

ing to y location, which describes the flame wrinkling and increase in flame surface area due to turbulence. Corresponding to Figs. 3 and 4, the quantities Ξ_d and Ξ_m are obtained from the DNS and the model, respectively, at different time and filter size. Figure 6 illustrates the comparison between Ξ_d and Ξ_m. It is evident that the magnitudes of actual and modeled integrated FSD agree very well. As seen from Figs. 3 and 4, the flame wrinkling exists mainly in the region of $0.004<y<0.015$ m. This leads to a high value of Ξ appearing in this region. With time evolution from $0.23t_e$ to $0.55t_e$,
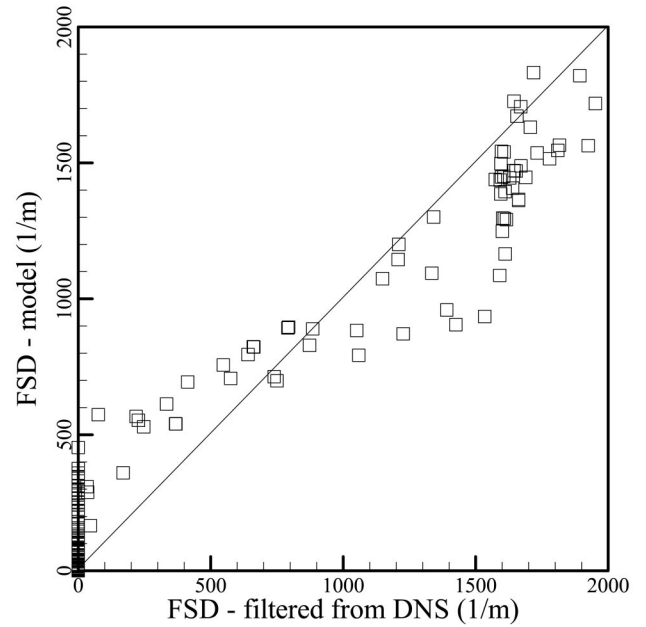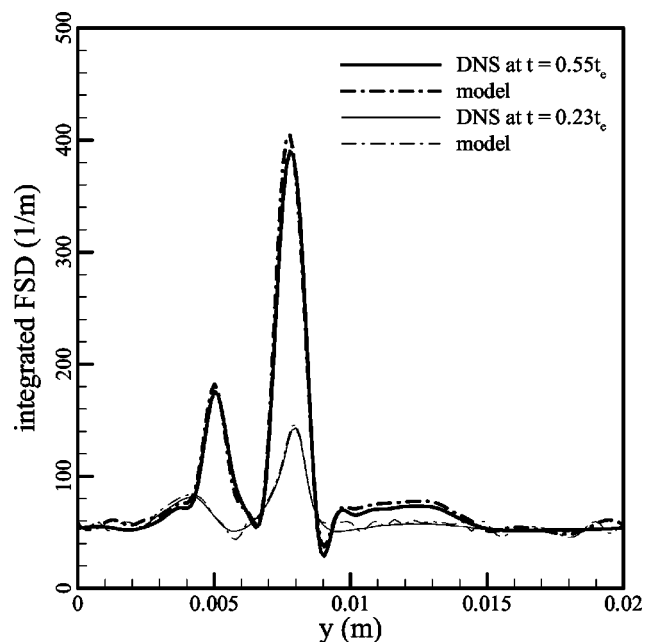
FIG. 6. Comparison of integrated FSD obtained from FSD model and from DNS data, plotted vs y location at $t=0.23t_e$ and $\Delta_f=8\Delta_x$, and $t=0.55t_e$ and $\Delta_f=16\Delta_x$, respectively.
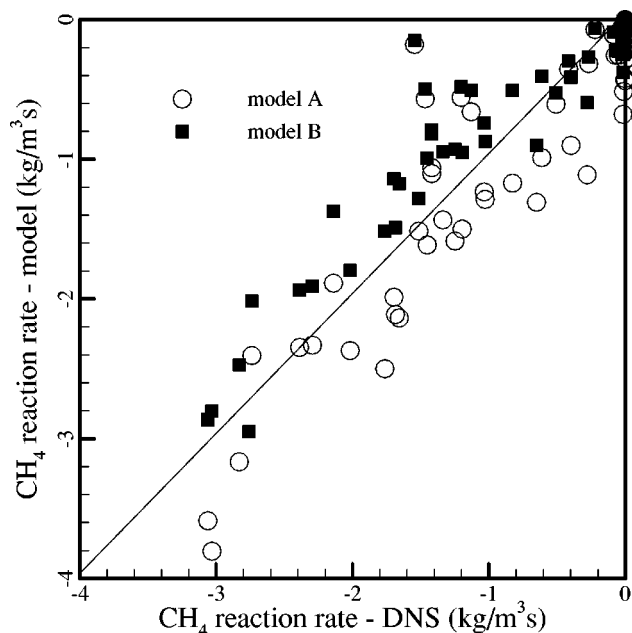
FIG. 7. Comparison of scatter plots of filtered reaction rate of CH_4: $m_{CH_4}(\bar{\chi}_{st})\bar{\Sigma}$ (model A) and $m_{CH_4}(\bar{\chi})\bar{\Sigma}$ (model B) from FSD model vs the exact one $\bar{\omega}_{CH_4}$ from DNS, at $t=0.55t_e$ and $\Delta_f=32\Delta_x$.

FIG. 8. Comparison of scatter plots of filtered reaction rate of H_2O: $m_{H_2O}(\bar{\chi}_{st})\bar{\Sigma}$ (model A) and $m_{H_2O}(\bar{\chi})\bar{\Sigma}$ (model B) from FSD model vs the exact one $\bar{\omega}_{H_2O}$ from DNS, at $t=0.55t_e$ and $\Delta_f=32\Delta_x$.

the value of Ξ increases rapidly. It indicates the increase of total flame area due to the distortion of turbulent motion. At other region, because the flame surface is not influenced strongly by turbulent motion, the value of Ξ remains almost a constant with time evolution. Because two filter sizes are used, it also means that integrated FSD is uninfluenced by filter size.

In general, the good agreement between the modeled FSD $\bar{\Sigma}_m(x,t)$, and the exact FSD $\bar{\Sigma}_d(x,t)$, suggests that the proposed model given by Eq. (36) is quite satisfactory. For the purpose of LES of nonpremixed turbulent flame, it is important to investigate the applicability of FSD concept to model the filtered reaction rate as reported in the following section.

B. Filtered reaction rate

The attractiveness of the FSD approach is that it decouples the complex chemical problem from the description of the turbulence combustion interaction by considering the flamelet consumption rate m_α and the filtered FSD $\bar{\Sigma}$, respectively. We now investigate this for filtered reaction rate. The effects of two proposed models for flamelet consumption rate $m_\alpha(\bar{\chi}_{st})$ [Eq. (41)] and $m_\alpha(\bar{\chi})$ [Eq. (51)] are also analyzed, where the former is referred to as model A and the latter as model B.

The flamelet consumption rate m_α of species α is estimated from a standard one-dimensional opposed laminar diffusion flame of pyrolysis fuel gas and air. The filtered FSD $\bar{\Sigma}(x,t)$ is estimated from Eq. (36). For reactant CH_4, Fig. 7 shows a scatter plot of the instantaneous reaction rates, $m_{CH_4}(\bar{\chi}_{st})\bar{\Sigma}$ (model A) and $m_{CH_4}(\bar{\chi})\bar{\Sigma}$ (model B) calculated from FSD model, versus the exact one $\bar{\omega}_{CH_4}$ obtained from DNS data. The time is $t=0.55t_e$ and the filter size is Δ_f

$=32\Delta_x$. Similarly, a scatter plot of instantaneous reaction rate of product H_2O is illustrated in Fig. 8 to compare with DNS data. Although the reaction rate of H_2O is more scattered, in general, the agreement between the exact and the modeled is reasonable and satisfactory. This demonstrates the applicability of FSD model in estimating the filtered reaction rate of reactants and products occurred in turbulent nonpremixed flame.

To compare the effect of model A and model B corresponding to the flamelet consumption rate, an error analysis is conducted by computing

$$\varepsilon_r = \left[\frac{\sum_1^N (r_{model} - r_{DNS})^2}{\sum_1^N (r_{DNS})^2} \right]^{1/2}, \tag{57}$$

which is the root mean square (rms) of errors normalized by the rms of the DNS values.[42] The errors ε_r from the models considered herein are 0.35 (model A) and 0.31 (model B) for reactant CH_4, and 0.77 (model A) and 0.65 (model B) for product H_2O. Because model B avoids the closure of the conditional average scalar dissipation rate, through which an error could be introduced, this error analysis shows better performance of model B over model A. For different filter size and other species, similar results can be obtained.

Further validation of the modeled reaction rate is carried out by examining the integrated values that are obtained by integrating across the flame along the x direction as conducted in Eq. (56). Figure 9 shows the integrated reaction rates of H_2O obtained from DNS and FSD model (models A and B), respectively, plotted versus y location. It is evident that model B provides a better agreement with the DNS data for integrated reaction rate.

In addition, another assessment is conducted in which the effects of SGS fluctuations in the filtered reaction rate are
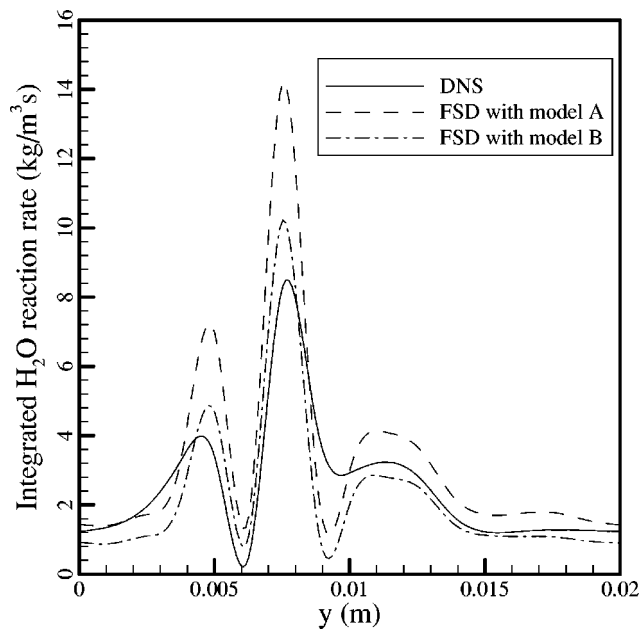
FIG. 9. Comparison of the integrated reaction rates of H_2O obtained from DNS and FSD model (model A and B) plotted vs y location.

ignored. It means the filtered reaction rate is calculated directly as $\bar{\omega}_\alpha(\Phi) = \omega_\alpha[\bar{\phi}(x,t)]$ without any subgrid reaction model, where ϕ stands for scalar vectors. For product H_2O, Fig. 10 shows a scatter plot of the instantaneous reaction rates, $m_{H_2O}(\bar{\chi})\bar{\Sigma}$ (FSD model) and $\omega_{H_2O}[\bar{\phi}(x,t)]$ (without FSD model), versus the exact one $\bar{\omega}_{H_2O}$ obtained from DNS data. The time is $t = 0.55\ t_e$ and the filter size is $\Delta_f = 16\ \Delta_x$. It is evident that the neglect of SGS effect results in significant over prediction of the reaction rate of H_2O. This will lead to
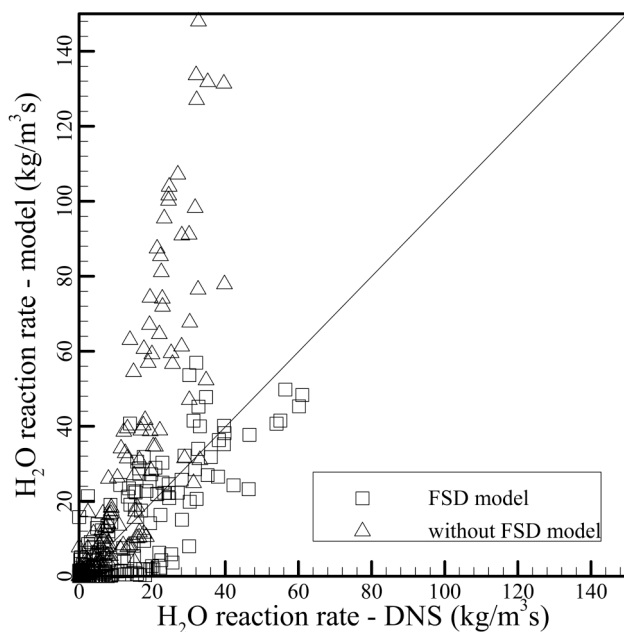
FIG. 10. Comparison of a scatter plot of the instantaneous reaction rates, $m_{H_2O}(\bar{\chi})\bar{\Sigma}$ (with FSD model) and $\omega_{H_2O}[\bar{\phi}(x,t)]$ (without FSD mode), vs the exact one $\bar{\omega}_{H_2O}$ obtained from DNS data, at $t = 0.55 t_e$ and $\Delta_f = 16\Delta_x$.
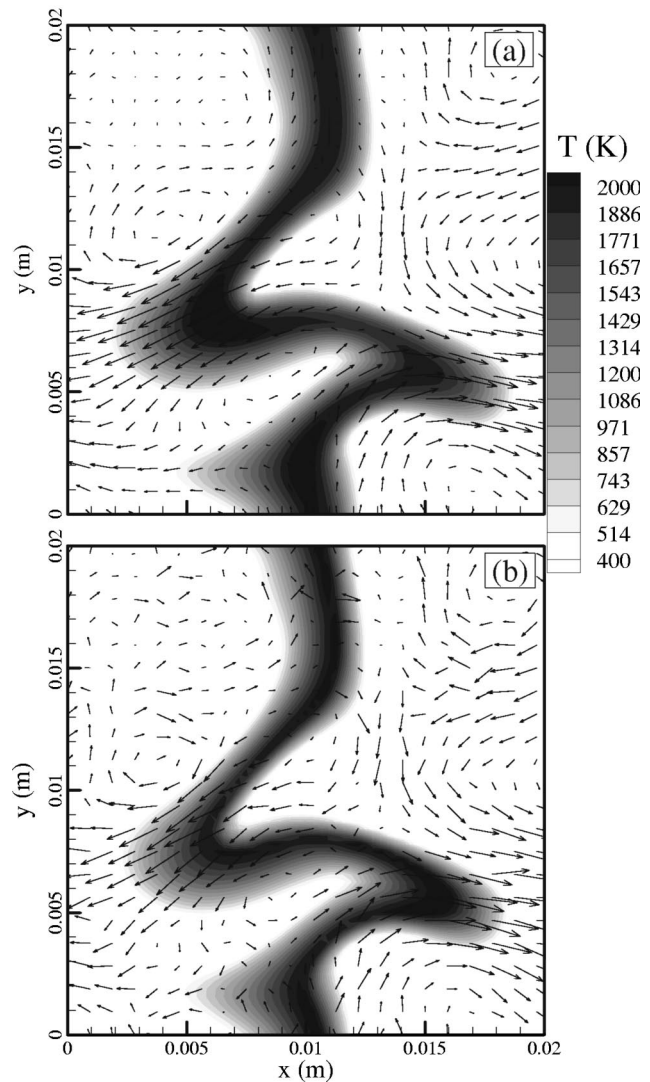
FIG. 11. Comparison of contours of instantaneous temperature and velocity vectors: (a) calculated from DNS; (b) calculated from 2D LES with the FSD model at time $t = 0.55 t_e$.

a higher production of H_2O. It suggests that the proposed FSD model provides a better description for the filtered reaction rate.

C. 2D LES computation

Using the same initial condition with DNS, a 2D LES computation with FSD model is conducted on a course grid, 65×65. Because the rates of energy production and species consumption in LES are greatly controlled by the combustion model, the LES results of calculated temperature and H_2O mass fraction are illustrated to assess the effect of FSD model. Figures 11(a) and 11(b) display a well-developed state of instantaneous contours of temperature and velocity vectors, obtained from DNS and LES, respectively, at time $t = 0.55 t_e$. With time evolution, the initially planar laminar flame illustrated by temperature profiles is stretched and distorted by the turbulence. In general, the temperature contours obtained from LES agree well with that from DNS. On the other hand, the turbulent intensity is considerably reduced by
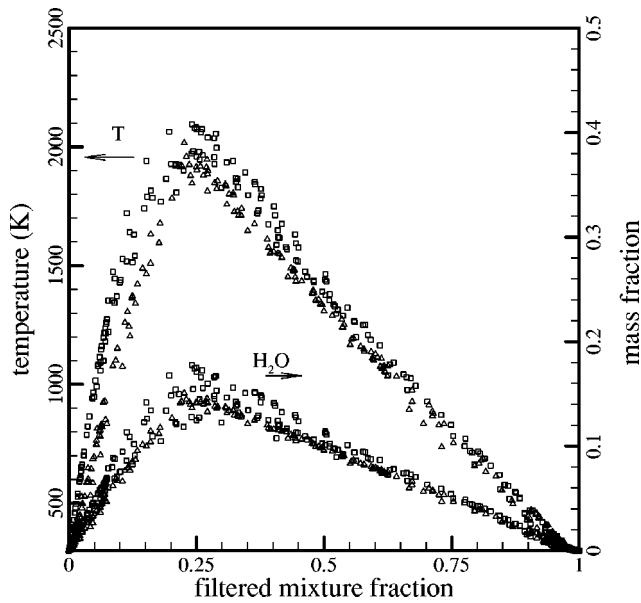
FIG. 12. Comparison of temperature and mass fraction of H_2O calculated from DNS (squares) and from 2D LES (triangles) with the FSD model at time $t=0.55t_e$.

FIG. 13. The instantaneous 3D contours of FSD computed from LES with the FSD model at time $t=0.3t_e$.

the enhanced viscous dissipation in the high temperature flame region. The velocity vectors shown in Fig. 11 illustrate the magnitude and direction of velocity in the computational domain. It shows a flow relaminarization occurs along the flame and the vorticity is weakened both due to an increase in kinematic viscosity with temperature and volumetric expansion. The velocity field calculated by LES is less smooth than DNS because a relatively coarse mesh size is utilized.

Figure 12 provides a quantitative comparison of temperature and mass fraction of H_2O obtained from DNS and from LES by using the proposed FSD model. The peak value of temperature computed by LES is a little lower than the prediction from DNS and the high temperature is concentrated in the region close to $\bar{Z}=Z_{st}$. This is expected since the FSD approach assumes that the total reaction and heat release process occur in the thin flamelet region. The mass fractions of H_2O computed by LES agree well with that of DNS. In general, the temperature and species mass fractions computed by LES with the FSD model agree well with the prediction from DNS data.

D. 3D LES computation

The time evolution of a plane laminar diffusion flame interacting with a 3D homogeneous and isotropic turbulent flow field is presented by a 3D LES computation in which the FSD-based turbulent combustion model is implemented. Because there is no 3D DNS data available at the present time, the applicability of the proposed FSD model to 3D LES computation is illustrated but not comparatively assessed.

Figure 13 shows the instantaneous 3D contours of FSD computed at time $t=0.3t_e$. With time evolution, the initially 2D planar laminar flame is stretched and distorted by a 3D turbulent flow. It displays a wave of peak and valley along the flame surface. This is more close to a real turbulent flame.
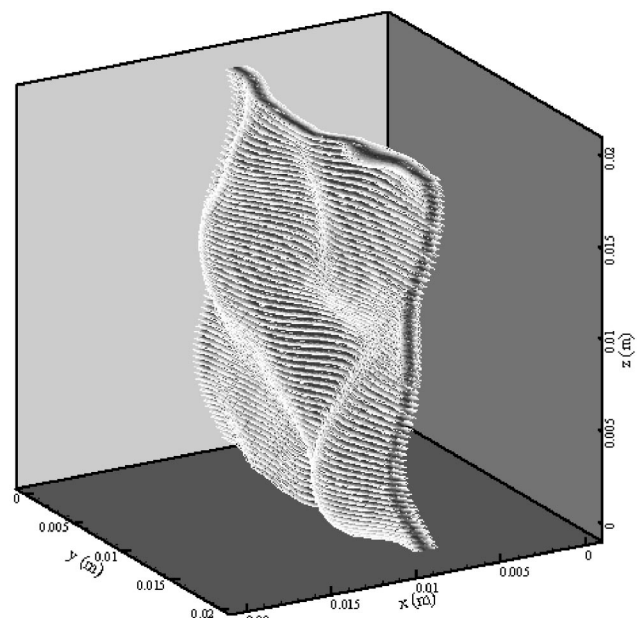
Figure 14 illustrates the temperature contours and velocity vectors at three interfaces along z direction. The velocity vectors illustrate the magnitude and direction of the 3D turbulent flow. In general, the temperature contours and magnitudes calculated from 3D LES are comparable with 2D LES calculations.

VI. CONCLUSIONS

It is demonstrated that the combustion model based on the flame surface density (FSD) concept provides a powerful method for large eddy simulation (LES) of turbulent nonpre-
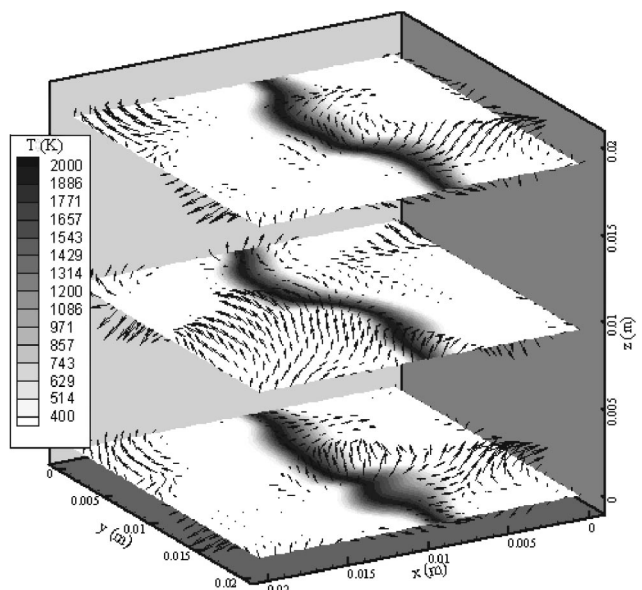
FIG. 14. The temperature contours and velocity vectors at three interfaces along z direction calculated from the 3D LES with the FSD model, at time $t=0.3t_e$.

mixed flame of wood pyrolysis gas and air. This method utilizes the advantage of FSD models that the complex chemical problem can be decoupled from the description of the turbulence combustion interaction. Model assessment is conducted through *a priori* and *a posteriori* analysis based on data from DNS of an initially unstrained laminar diffusion flame of wood pyrolysis gas evolving in a decaying isotropic and homogeneous turbulence.

For LES, although an exact equation for the filtered FSD may be derived, modeling of unclosed terms that arise is difficult. An alternate approach is developed in this paper in which the filtered FSD is modeled as a product of the gradient of mixture fraction and the filtered probability density function. This concept is validated from DNS data using spatial filtering operation. Results show that the proposed FSD model provides a good description for the filtered flame surface density. Using the flame surface density concept, the filtered reaction rate of species is modeled as the product of the flamelet consumption rate m_α and the filtered FSD $\bar{\Sigma}$. It is found that complex chemistry can be used in the FSD approach with an acceptable accuracy.

Two models (A and B) for flamelet consumption rate m_α are proposed to consider the effect of filtered scalar dissipation rate. The analysis on the flamelet consumption rate indicates that the accuracy of FSD model can be improved by improving model of m_α, in which (model B) m_α is only controlled by the scalar dissipation rate but avoids the closure of the conditional average value. This assumption needs more analysis and over a range of conditions. In the future, a three-dimensional LES of turbulent nonpremixed flame of wood pyrolysis gas over a larger physical domain coupled with FSD model will be developed and applied in a real fire problem.

ACKNOWLEDGMENTS

[1] P. Givi, "Model free simulation of turbulent reactive flows," Prog. Energy Combust. Sci. **15**, 1 (1989).

[2] S. Mahalingam, J. H. Chen, and L. Vervisch, "Finite-rate chemistry and transient effects in direct numerical simulations of turbulent nonpremixed flames," Combust. Flame **102**, 285 (1995).

[3] L. Vervisch and T. Poinsot, "Direct numerical simulation of nonpremixed turbulent flame," Annu. Rev. Fluid Mech. **30**, 655 (1998).

[4] D. Veynante and L. Vervisch, "Turbulent combustion modeling," Prog. Energy Combust. Sci. **28**, 193 (2002).

[5] U. Schumann, "Large eddy simulation of turbulent diffusion with chemical reactions in the convective boundary layer," Atmos. Environ. **23**, 1713 (1989).

[6] P. A. McMurty, S. Menon, and A. R. Kerstein, "A linear eddy sub-grid model for turbulent reacting flows: Application to hydrogen-air combustion," Proc. Combust. Inst. **24**, 271 (1992).

[7] C. Fureby and C. Lofstrom, "Large-eddy simulations of bluff body stabilized flames," Proc. Combust. Inst. **25**, 1257 (1994).

[8] N. Branley and W. P. Jones, "Large eddy simulation of a turbulent nonpremixed flame," Combust. Flame **127**, 1914 (2001).

[9] N. Peters, "Laminar diffusion flamelet models," Prog. Energy Combust. Sci. **10**, 319 (1984).

[10] A. W. Cook, J. J. Riley, and G. Kosaly, "A laminar flamelet approach to subgrid-scale chemistry in turbulent flow," Combust. Flame **109**, 332 (1997).

[11] S. M. de Bruyn Kops, J. J. Riley, and G. Kosaly, "Investigation of modeling for non-premixed turbulent combustion," Flow, Turbul. Combust. **60**, 105 (1998).

[12] P. E. DesJardin and S. H. Frankel, "Large eddy simulation of a nonpremixed reacting jet: Application and assessment of subgrid-scale combustion models," Phys. Fluids **10**, 2298 (1998).

[13] S. B. Pope, "PDF methods for turbulent reactive flows," Prog. Energy Combust. Sci. **11**, 119 (1985).

[14] F. Gao and E. E. O'Brien, "A large-eddy simulation scheme for turbulent reacting flows," Phys. Fluids A **5**, 1282 (1993).

[15] P. J. Colucci, F. A. Jaberi, P. Givi, and S. B. Pope, "Filtered density function for large eddy simulation of turbulent reacting flows," Phys. Fluids **10**, 499 (1998).

[16] F. A. Jaberi, P. J. Colucci, S. James, P. Givi, and S. B. Pope, "Filtered mass density function for large-eddy simulation of turbulent reacting flows," J. Fluid Mech. **401**, 85 (1999).

[17] A. Y. Klimenko, "Multicomponent diffusion of various admixtures in turbulent flow," Fluid Dyn. **25**, 327 (1990).

[18] R. W. Bilger, "Conditional moment closure for turbulent reacting flow," Phys. Fluids A **5**, 436 (1993).

[19] W. K. Bushe and H. Steiner, "Conditional moment closure for large eddy simulation of non-premixed turbulent reacting flows," Phys. Fluids **11**, 1896 (1999).

[20] F. Marble and J. Broadwell, "The coherent flame model of non-premixed turbulent combustion," Project Squid TRW-9-PU, Project Squid Headquarter, Chaffee Hall, Purdue University, 1977.

[21] S. B. Pope, "The evolution of surfaces in turbulence," Int. J. Eng. Sci. **26**, 445 (1988).

[22] L. Vervisch, E. Bidaux, K. N. C. Bray, and W. Kollmann, "Surface density function in premixed turbulent combustion modeling, similarities between probability density function and flame surface approaches," Phys. Fluids **7**, 2496 (1995).

[23] E. Van Kalmthout and D. Veynante, "Direct numerical simulations analysis of flame surface density models for nonpremixed turbulent combustion," Phys. Fluids **10**, 2347 (1998).

[24] M. Boger, D. Veynante, H. Boughanem, and A. Trouve, "Direct numerical simulation analysis of flame surface density concept for large eddy simulation of turbulent premixed combustion," Proc. Combust. Inst. **27**, 917 (1998).

[25] R. O. S. Prasad and J. P. Gore, "An evaluation of flame surface density models for turbulent premixed jet flames," Combust. Flame **116**, 1 (1999).

[26] E. R. Hawkes and R. S. Cant, "Implications of a flame surface density approach to large eddy simulation of premixed turbulent combustion," Combust. Flame **126**, 1617 (2001).

[27] X. Zhou and S. Mahalingam, "A flame surface density based model for large eddy simulation of turbulent nonpremixed combustion," Phys. Fluids **14**, 77 (2002).

[28] P. Morf, P. Hasler, and T. Nussbaumer, "Mechanisms and kinetics of homogeneous secondary reactions of tar from continuous pyrolysis of wood chips," Fuel **81**, 843 (2002).

[29] X. Zhou and S. Mahalingam, "Evaluation of reduced mechanism for modeling combustion of pyrolysis gas in wildland fire," Combust. Sci. Technol. **171**, 39 (2001).

[30] P. Moin, K. Squires, W. Cabot, and S. Lee, "A dynamic subgrid-scale model for compressible turbulence and scalar transport," Phys. Fluids A **3**, 2746 (1991).

[31] G. A. Bird, *Molecular Gas Dynamics and the Direct Simulation of Gas Flows* (Clarendon, Oxford, 1994).

[32] *Large Eddy Simulations of Complex Engineering and Geophysical Flows*, edited by B. Galperin and S. A. Orszag (Cambridge University Press,

Cambridge, 1993).

[33]R. J. Kee, F. M. Rupley, and J. A. Miller, "CHEMKIN-II: A fortran chemical kinetics package for the analysis of gas-phase chemical kinetics," Sandia National Laboratories Report No. SAND89-8009B.

[34]S. B. Pope, "Computations of turbulent combustion: Progress and challenges," Proc. Combust. Inst. **23**, 591 (1990).

[35]X. Zhou and S. Mahalingam, "A suitable mixture fraction for diffusion flames of wood pyrolysis gas," Combust. Flame **133**, 197 (2003).

[36]L. Guichard, and L. Vervisch, "Development of a high order code for solving Navier–Stokes equations, Study of shock vortex interaction within a mixing zone," LMFN-CORIA No. 1993-25, 1993.

[37]S. K. Lele, "Compact finite difference schemes with spectral-like resolution," J. Comput. Phys. **103**, 16 (1992).

[38]W. Pakdee and S. Mahalingam, "An accurate method to implement boundary conditions for reacting flows based on characteristic wave analysis," Combust. Theory Modell. **7**, 705 (2003).

[39]T. J. Poinsot and S. K. Lele, "Boundary conditions for direct simulations of compressible viscous flows," J. Comput. Phys. **101**, 104 (1992).

[40]M. Baum, T. Poinsot, and D. Thevenin, "Accurate boundary conditions for multicomponent reactive flows," J. Comput. Phys. **116**, 247 (1994).

[41]F. G. Jacobitz, "Efficiency of parallel direct numerical simulations of turbulent stratified shear flow," AIAA Paper 2003-0077, 2003.

[42]C. Wall, B. J. Boersma, and P. Moin, "An evolution of assumed beta probability density function subgrid-scale model for large eddy simulation of nonpremixed turbulent combustion with heat release," Phys. Fluids **12**, 2522 (2000).